LA-UR -87-1478

CONF-8705104--2

Los Alamos National Laboratory is operated by the University of California for the United States Department of Energy under contract W-7405-ENG-36

LA-UR--87-1478

DE87 010097

TITLE: MICROSTRUCTURAL ASPECTS OF SPALLATION IN COPPER

AUTHOR(S): A. Zurek and C. Frantz

SUBMITTED TO Proceedings of "Impact 87", An International Conference on Impact Loading and Dynamic Behavior of Materials in Bremen, West Germany, May 18-22, 1987.

DISCLAIMER

Los Alamos Los Alamos National Laboratory
Los Alamos, New Mexico 87545

Microstructural Aspects of Spallation in Copper

A. K. Zurek and C. E. Frantz, Los Alamos National Laboratory, Los Alamos, New Mexico, U.S.A., 87545

Introduction

Compressive shock waves, used extensively in a number of experimental areas, result in a specific kind of fracture called a spall, which is caused by development of tensile stresses during the interaction of opposing release waves. In copper, ductile tensile failure is generated under an explosive pulse load (1-3), but the stress at which this material fails depends on its preconditioning, which has determined its grain size, and its purity, and on its prior shock state of deformation (4-8).

The metallurgical aspects of copper spalling and crack or void initiation sites, the effects of grain size and substructure, and the micromechanical aspects of growth and coalescence have not received the detailed attention that other deformation phenomena have received. The most complete accounts of metallurgical effects to date are those provided by Shockey et al. (7) in 1973 and by Curran and Seaman in 1987 (9), and even these do not cover all of the variables mentioned above.

The present work was stimulated by the observation that under identical shock loading conditions the spall strength of copper can vary between 0.4 to 2.4 GPa -- an unusually wide range -- merely as a result of changes in its microstructure.

Examples of fracture morphology are presented and possible micromechanics of fracture resulting from different microstructures are discussed. Finally, the implications of these observations on modeling are presented.

Experimental Method

Disc specimens cut from bars of 10100 Cu and 99.95%-commercial purity (ETP) Cu, annealed to give average grain sizes of 200 and 40 μm, respectively, were subjected to planar impact in a 40 mm gas gun. The specimen and flyer geometries and dimensions are shown in Fig. 1. All specimens were impacted with a flat flyer at velocities of approximately 425 m/s, producing a shock wave of 8 GPa pressure and 1 μs duration. To obtain a flat-on-impact, the specimens were aligned with a laser beam, and the gun system was evacuated at the time of impact. Impacted specimens were recovered using a specially designed soft recovery catcher tank to ensure minimal damage to the fracture surfaces (10). The ultrasonically cleaned spall surfaces and cross sections of these spall surfaces were examined by stereo-scanning electron microscopy. Cross sections of spall surfaces were obtained by sectioning samples in half and electropolishing the cut surfaces while the actual spall fracture surface was carefully preserved using microstop. In each test, impact pressure and spall strength were measured using two manganin gauges in separate pulsed Wheatstone bridge circuits in conjunction with a specially designed delayed triggering system to ensure a high signal-to-noise ratio. A typical observed

stress history is shown in Fig. 2, where resistance, R_1, is related to the impact pressure, and spall strength is related to resistance, R_2 (11). Table 1 presents the average spall strength for each condition of the coppers.

COPPER	GRAIN SIZE [μm]	SPALL STRENGTH [GPa]
10100	40 200	2.4 1.5
COMMERCIAL COPPER	40 200	1.5 0.4

TABLE I. Measured Spall Strength Using Manganin Gauges vs. Copper Purity and Grain Size

Spall Fracture of High-Purity Copper

The spall strength of high-purity 10100 copper ranges from 1.5 to 2.4 GPa and depends on the grain size. The small-grained 10100 Cu showed the highest spall strength, 2.4 GPa, while copper with 200 μm grains spalled at a 1.5 GPa tensile stress. The spall of 200 μm grain 10100 Cu occurs primarily along the grain boundaries as is shown (Fig. 3) on the cross-sectional view of the spall surface. The grain boundary voids grow and coalesce to form what appear to be large facets around isolated islands of transgranular microvoids, as shown in Fig. 4. This planar, transgranular voiding (Fig. 5) is entirely homogeneous, resembling the homogeneous, single-crystal voiding reported in the early 1970s by Stevens et al. (12). In each spherical void there is an octahedral-shaped feature, most likely the void nucleation site. No other deformation except the grain boundary voiding and transgranular microvoiding is observed on either the cross-section view or the actual spall surface.

The spall surface view (Fig. 6) of the 40 μm grain 10100 copper is very similar to that of 200 um grain material. However, no obvious facets are present; consequently, the spall surface is smoother. The cross section of the fracture surface revealed slip bands and twins within single grains, which are evidence of large deformation (Fig. 7). The transmission electron microscopy obtained from the cross section of the region just under the spall surface confirmed the presence of twins, slip bands, and additional dislocation cells and dislocation tangles. Voids are formed at the cross slips of deformation bands. Only occasionally, when a large grain is encountered, does voiding proceed along the boundaries of the grain, as shown in Fig. 7.

Spall Fracture in Commercial-Purity Copper

The spall strength of commercial-purity copper is appreciably lower than that of high-purity oxygen-free 10100 copper and ranges from 0.4 GPa for large grain size to 1.5 GPa for small grain size. The CuO inclusions in this material are relatively randomly distributed. However, occasional clustering is also found. In both 40 μm and 200 μm grain material, voiding occurs mainly around the inclusions (Fig. 8). Void size as well as distribution correlates with the distribution of the particles. The fracture surface is smooth and no facets are present, Fig. 9. Cross sections show that indeed voiding is as random as the distribution of particles. However, final spall fracture follows the shape of the deformation cells (Fig. 10), which is very clearly observable in stereo imaging in contrast to planar projection.

Discussion

Several attempts have been made to model dynamic fracture, particularly the spallation process in ductile material. McClintock (5) models the spall fracture by hole growth, where parameters such as dislocation viscosity, adiabatic heat generated locally at shock, thermal diffusivity, and mechanical inertia play important roles in the model. He discusses the different roles of parameters at different load intensities in such materials as Cu, Al, and Fe alloys. Jones and Dawson (6) discuss in a qualitative manner the influence of metallurgical parameters such as dislocation densities, stacking fault energies, and the state of precipitation on the dynamic fracture. They show that when the dislocation density increases, the dynamic fracture strength of ductile material increases while total induced strain decreases. Decreasing the stacking fault energy by alloying (for instance Cu with Al 7%) also increases the dynamic fracture strength and the twin density resulting from the impact. They also observed an increased level of spall damage with increasing aging time, which controls the state of precipitations in the material. Shockey et al. (7) analyzed qualitatively the influence of microstructural features on dynamic fracture. Brandon et al. (3) reported an inverse relationship between the purity of copper and its final spall strength. Their experiments were performed on slightly larger samples and at much lower stresses which would lead to lower strain rates. These conditions apparently changed the spall mechanism from that observed in our experiments. Additionally, their samples were cut from rolled material, and the final fracture surface was significantly influenced by prior sample rolling.

In our work we limited the number of material parameters to very basic ones, grain size and purity, while keeping the shock parameters constant. We hope this approach simplifies the problem enough to facilitate some basic understanding and consequently modeling of spalling.

The observations made in our experiments are generally consistent with those previously reported (1,7), but contain important additional information. For example, the spall strength in the void growth model used by Johnson (13) to represent the tensile fracture behavior of OFHC copper (2) is given by

$$\sigma_s = (2Y/3) \ln \phi_0 \qquad \text{Equ. 1}$$

where Y is the elastic-plastic flow strength of the material surrounding the growing voids and ϕ_0 is the initial porosity: Y = 0.25 GPa and ϕ = 0.0003 for copper. This gives σ_s = 1.4 GPa, in near agreement with the measured value of 1.5 GPa for commercial copper (40 μm grain size). The void-growth model assumes the pre-existence of a small amount of porosity from which the spherical voids grow.

The experimental data presented here exhibit several additional important rules. The first is that standard copper, containing numerous CuO inclusions, fractures by means of void growth from pre-existing sites, i.e., the spall is void-growth and coalescence controlled. This material should then be adequately represented by the simple void-growth model. The effect of grain size enters in Equ. 1 through the flow strength Y which vary with grain size. However, the flow-stress variation with grain size is expected to be much less than the ratio of the spall strength measured experimentally. Hence, the theoretical variation in spall strength is only qualitatively correct.

In the case of pure (10100) copper, the fracture process is more complicated. We believe that especially in the case of 200 μm grained 10100 Cu, the spall is controlled by void nucleation. There is also competition between void growth originating from grain boundaries and from voids nucleated (apparently homogeneously) within individual crystal grains. Initial void formation occurs by diffusion of vacancies along the grain boundaries rather than via inner grain diffusion (14). That is, the vacancies for void growth are produced by the tension across the grain boundaries rather than by deformation inside the grain. This mechanism is consistent with the observation that the grains did not show any deformation and suggests that the creep mechanism is responsible for the grain boundary void formation in 200 μm 10100 Cu. The homogeneous nucleation across the grains is similar to that described by Stevens et al. (12), where dislocations initially slip along (111) crystal planes to form octahedral features, and then void growth proceeds in a less stable manner to form the usually observed spherical ductile dimples. The magnitudes of the relative contributions from both nucleation mechanisms to the overall fracture process depend on the grain size: for small grains the crystalline contribution becomes more important. A spallation model for this material would require the summation of two terms to the void-growth-rate expression:

$$d\phi/dt = d\phi_g/dt + d\phi_h/dt \quad , \qquad \text{Equ. 2}$$

with ϕ_g and ϕ_h being porosities arising from grain boundary and homogeneous contributions, respectively. In this model, the initial porosity associated with the grain boundaries is assumed to be pre-existent while the crystalline contribution nucleated according to an expression of the form

$$dN/dt = \dot{N}_0 \exp(|\sigma|/\sigma_0) \qquad \text{Equ. 3}$$

where σ is the tensile stress component and $\dot{N}_0$ and σ_0 are constants. The experiments here show that the grain boundary contribution to spallation increases with increasing grain size (the 200 μm material shows a lower spall strength), and this would also have to be accounted for.

The behavior of pure copper is clearly more complicated than that of standard copper containing CuO impurities. It is only through careful pre- and post-shot microscopic examination that the individual contributions can be uniquely determined.

Acknowledgements

This work has been sponsored by the U. S. Air Force Armament Laboratory under Contract No. DE-AI04-79AL 11812 and has been performed under the auspices of the United States Department of Energy. The authors would like to thank Marvin Anstey and Benito Jacquez for their technical support in the experimental part of this research, and we thank Rusty Gray for performing the transmission electron microscopy.

References

(1) L. Seaman, T. W. Barbee, Jr., D. R. Curran: "Dynamic Fracture Criteria for Homogeneous Materials," SRI Technical Report No. AFWL-TR-71-156 (1971).
(2) T. W. Barbee, Jr., L. Seaman, R. Crewdson, D. R. Curran: J. of Materials, 7, No. 3 (1972) 393-401.
(3) D. G. Brandon, M. Boas, Z. Rosenberg: "Effect of Grain Boundaries on Ductile Fracture Under Planar Impact," Institute Phys. Conf. Ser. No. 70 (1984) 261-268.
(4) A. V. Granato: "Metallurgical Effects at High Strain Rates," R. W. Rohde, B. M. Butcher, Eds., Plenum Press, New York (1973) 255.
(5) J. A. McClintock: "Metallurgical Effects at High Strain Rates," R. W. Rohde, B. M. Butcher, Eds., Plenum Press, New York (1973) 415.
(6) W. B. Jones, H. I. Dawson: "Metallurgical Effects at High Strain Rates," R. W. Rohde, B. M. Butcher, Eds., Plenum Press, New York (1973) 443.
(7) D. A. Shockey, L. Seaman, D. R. Curran: "Metallurgical Effects at High Strain Rates," R. W. Rohde, B. M. Butcher, Eds., Plenum Press, New York (1973) 473.
(8) W. C. Leslie: "Metallurgical Effects at High Strain Rates," R. W. Rohde, B. M. Butcher, Eds., Plenum Press, New York (1973) 571.
(9) D. R. Curran, L. Seaman: "Dynamic Failure of Solids," Physics Reports (Review Section of Physics Letters), in press.
(10) C. E. Frantz, G. T. Gray: "A Water Catch System Inside an Evacuated Catch Tank of a 40 mm Gun System," presented at and in Proceedings of Aeroballistic Range Association Meeting, Quebec, Canada, Sept. 9-12 (1986).
(11) V. I. Romanchenho and G. V. Stepanov: Zhurnal Prikladnoi Mekhaniki i Technicheskoi Fiziki (translation) No. 4 (1980) 141-147.
(12) A. L. Stevens, Lee Davison, W. E. Warren: J. Appl. Phys., 43, No. 12 (1972) 4922-4927.
(13) J. N. Johnson: J. Appl. Phys. 52(4) (1981) 2812-2825.
(14) D. Hull, D. E. Rimmer: Phil. Mag. Ser. 8, 4 (1959) 673-687.

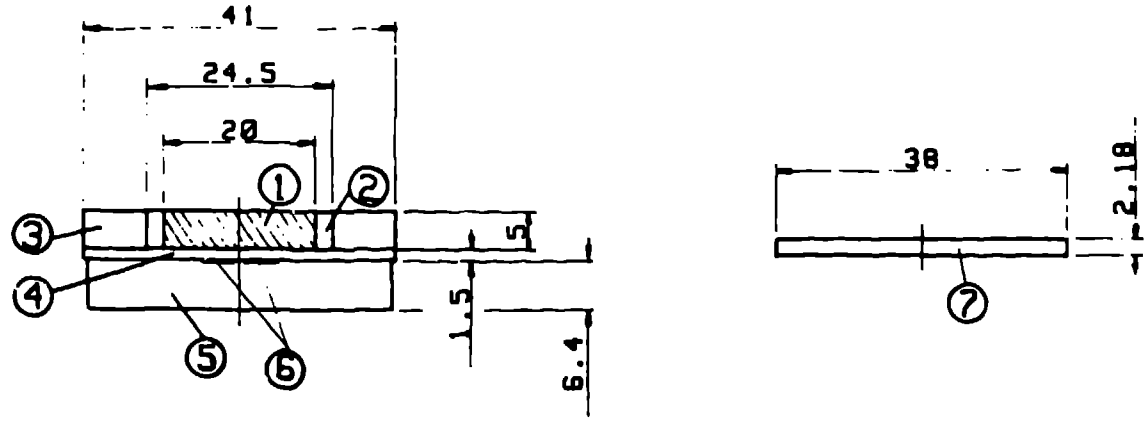

Fig. 1: Specimen and flyer plate geometries and dimensions: (1) and (7) are the copper sample and the copper flyer plate, respectively; (2) and (3) are the copper guarding rings designed to trap radial release waves. (4) and (5) are plexiglas backing plates between which manganin gauges (6) are sandwiched.

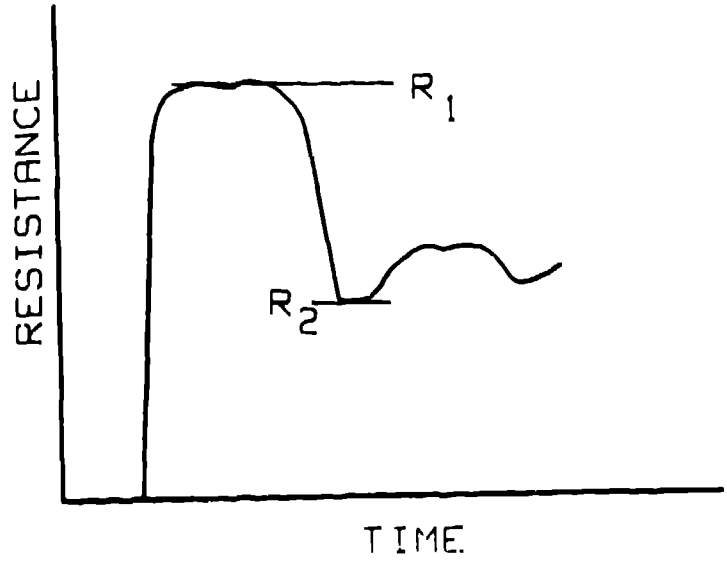

Fig. 2: A typical stress history obtained from manganin gauge measurement of resistance [volts] vs. time [s].

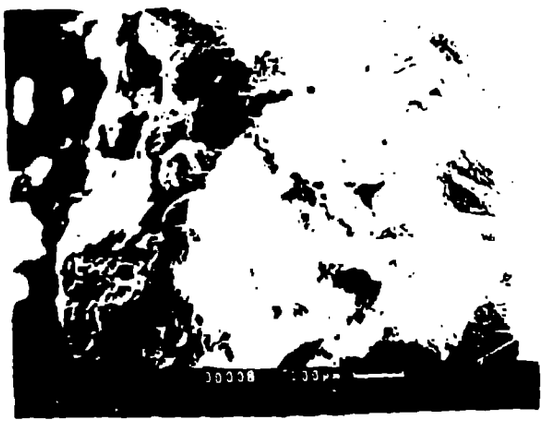

Fig. 3: Cross-sectional view of 200 m grain 10100 Cu. Note the grain boundary voiding. The Actual spall surface runs vertically on the left-hand side of the micrograph.

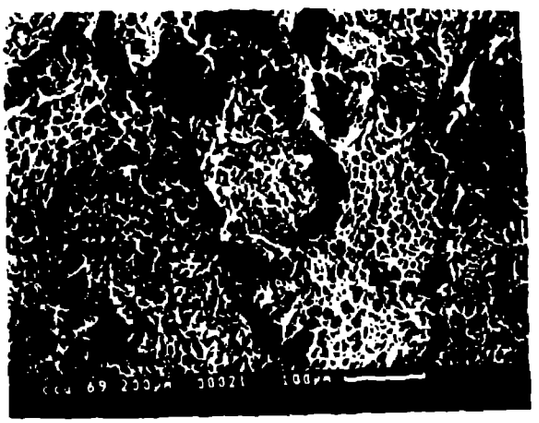

Fig. 4: Spall surface of 200 m grain 10100 Cu. Large facets are clearly visible around transgranular microvoids.

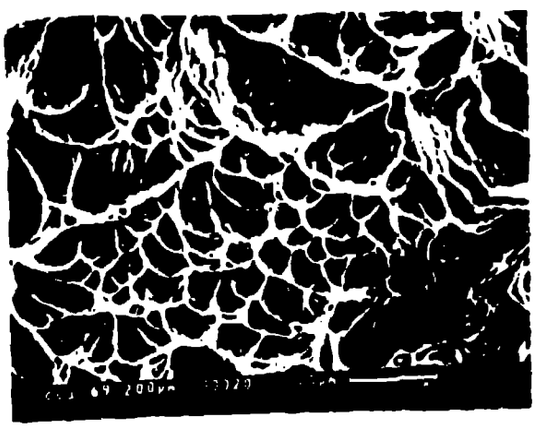

Fig. 5: Spall surface of 200 m grain 10100 Cu. The micrograph shows homogeneous transgranular voiding.

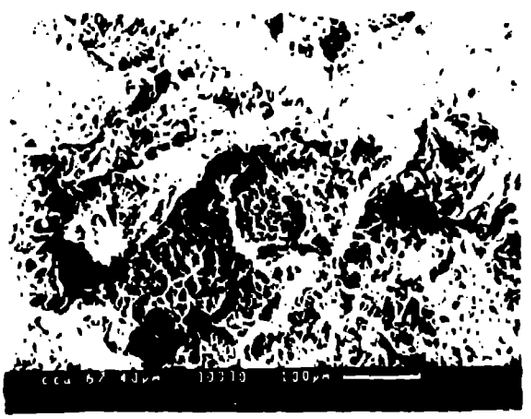

Fig. 6: Low magnification of the spall fracture surface of 40 m grain 10100 Cu.

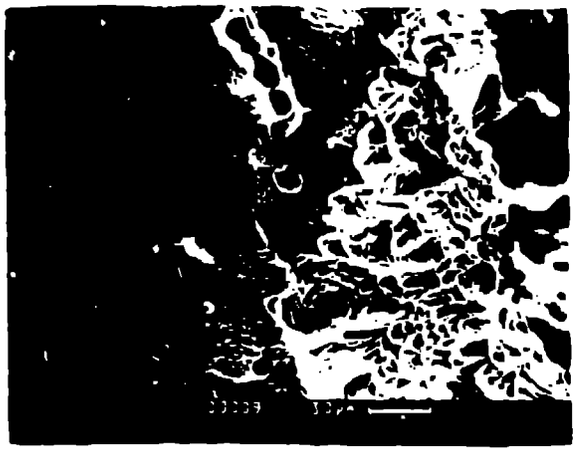

Fig. 7: Cross-sectional view of 40 m grain 10100 Cu. Shown are deformation cells with slip bands and twins and voiding along the grain boundary of a large grain. The spall surface runs vertically on the right-hand side of the micrograph.

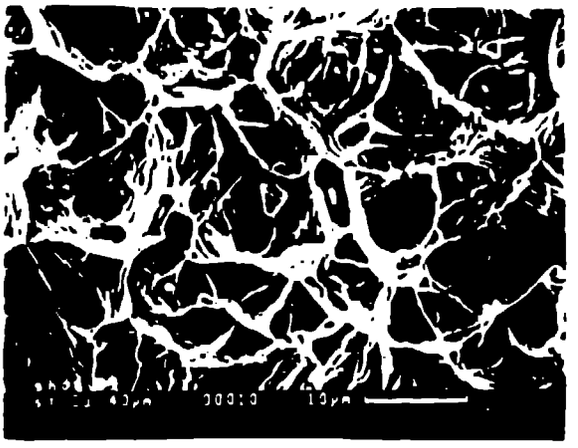

Fig. 8: Spall surface of 200 m grain commercial OFHC copper. Shown are spherical voids with CuO inclusions in their centers.

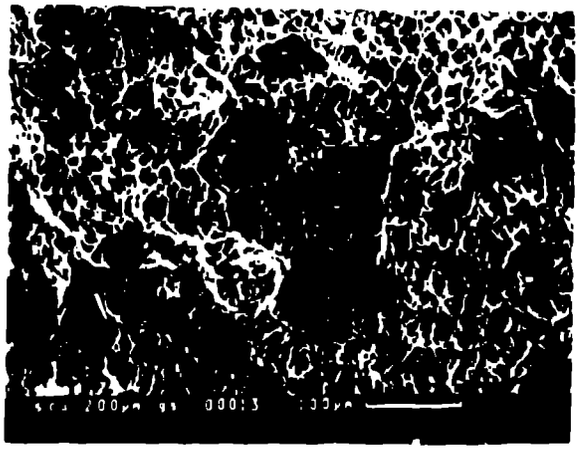

Fig. 9: Low magnification of spall fracture surface of 40 m grain commercial OFHC copper.

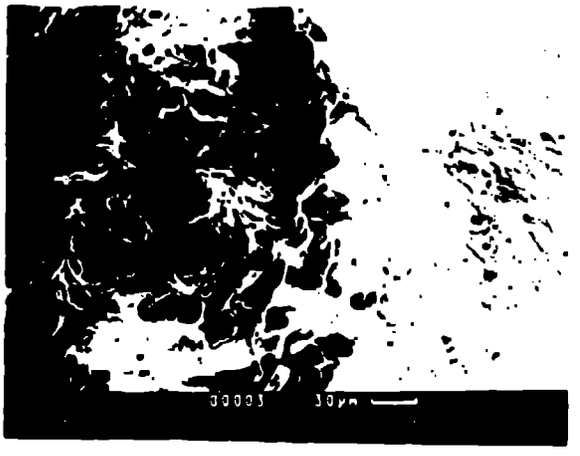

Fig. 10: Cross-sectional view of 200 m grain commercial OFHC copper. The spall surface runs vertically on the left-hand side of the micrograph.